Electronic Supplementary Information

Promoted Alkaline Hydrogen Evolution by N-doped Pt-Ru Single Atoms Alloy

Mi Luo,[†a] Jinyan Cai,[†b] Jiasui Zou,[†a] Zheng Jiang,[c,d] Gongming Wang,[b] and Xiongwu Kang,[*a]

[a] New Energy Research Institute, School of Environment and Energy, South China University of Technology, Higher Education Mega Center, 382 East Waihuan Road, Guangzhou 510006, China.

E-mail: esxkang@scut.edu.cn

[b] Hefei National Laboratory for Physical Sciences at the Microscale and Department of Chemistry, University of Science & Technology of China, 230026 Hefei, Anhui, China.

[c] Shanghai Advanced Research Institute, Chinese Academy of Sciences, Shanghai 201210, China

University of Chinese Academy of Sciences, Beijing 100049, China

[†] The authors contribute equally to this work

*Corresponding authors

1. Experimental details

1.1 Materials

Chloride hexahydrate ($RuCl_3$, 99%, Energy Chemical), chloroplatinic acid hexahydrate ($H_2PtCl_6 \cdot 6H_2O$, Energy Chemical), sodium borohydride($NaBH_4$, Energy Chemical), multi-walled carbon nanotubes (CNTs,＞97%), Pd/C commercial catalyst (10 wt%, Alfa Aesar) were used as received. Ethanol (CH_3CH_2OH, 99%), and sodium hydroxide (NaOH, 96%) were purchased from Sinopharm Chemical Reagent Co. Ltd. and used directly.

1.2. Structure Characterizations

Morphologies and microstructures of all samples were examined by field-emission scanning electron microscope (FESEM, Hitachi S4800), TEM (JEOL 2100F) and SACTEM. The powder X-ray diffraction (XRD) of the alloy NPs were performed on a Bruker D8 Advance powder X-ray diffractometer using a Cu-Kα source (λ= 0.154059 nm, 2θ range of 10-90° and a scan rate of 10° min^{-1}). The surface chemical composition of the samples was analyzed by X-ray photoelectron spectroscopy (XPS), an ESCALAB_250Xi X-ray photoelectron spectrometer with an Mg Kα source.

1.3. Synchrotron Radiation based characterization

The Pt L_3-edge (11564 eV) and Ru K-edge (22117 eV) X-ray absorption fine structure (XAFS) spectra were measured in transmission mode at beamline BL14W1 of the Shanghai Synchrotron Radiation Facility (SSRF), China.[1] The storage rings were operated at 3.5 GeV with a 230 mA electron beam current. The beamline was

monochromatized with a double-crystal monochromator (DCM) equipped with Si(111) crystals and the beam size at the samples was approximately 300 mm×300 mm (FWHM). A transmission XANES spectrum was recorded from a metallic Pd reference foil and used to provide an accurate energy calibration for all Ru K-edge spectra. The first inflection point of the Ru-K edge was set to 21817 eV, and the integration time for different energy intervals was 1s. Each spectrum was recorded over about 16 min with an unfocused beam. All XAFS spectra were analyzed using the Demeter software package (University of Chicago).[2] The XANES raw data were normalized by a procedure consisting of several steps.[3] First, the photon energy was calibrated based on the Pt 5f and Ru 5f peak of a freshly sputtered gold wafer, respectively and then using a substrate line to set the pre-edge at zero. Finally, the spectra were normalized to yield an edge-jump to one. For each fitting, the theoretical curved-wave backscattering amplitude ($F_j(k)$), phase-shift functions ($\phi_j(k)$) and the mean free path in Å(l) of all the paths were calculated by FEFF8.2 code (University of Washington).[4] Each model was set up based on the known crystal structure.[5]

1.4. Electrochemical measurements

The HER performance of the as-prepared catalysts was evaluated on the electrochemical workstation (CH Instrument 1760E) with a standard three-electrode setup in 1.0 M KOH aqueous solution. The Hg/HgO electrode and a graphite rod were used as the reference and counter electrode, respectively. The working electrode is the as-prepared samples. To remove the dissolved oxygen, the electrolyte was purified with

N_2 bubble for 30 min before test. The final potential was calibrated to the reversible hydrogen electrode (RHE) according to the following equation: E(vs. RHE) = E(vs. Hg/HgO) + E^0(Hg/HgO) +0.059 × pH in the 1.0 M KOH. Linear sweep voltammetry (LSV) tests were carried out to examine the electrochemical activity of these electrodes with a scan rate of 1 mV s^{-1}. The Tafel slopes were obtained based on the LSV plots. Electrochemical impedance spectra (EIS) were recorded with an AC amplitude of 10 mV. The frequency ranged from 10 kHz to 0.1 Hz, and the polarization voltage was -0.35 V versus SCE. All these results were obtained by iR compensation.

1.5. Theoretical Calculations

The DFT calculations performed here were carried out using the CASTEP program in Material Studio 8.0.[6] Perdew-Burke-Ernzerhof (PBE) of the generalized gradient approximation (GGA) was used to treat the electron exchange and correlation. To describe the interaction between valence electrons and ionic core, ultrasoft pseudopotentials (USP) was applied. The wave function of the valence electronic states was expanded in the plane-wave basis set with the energy cutoff of 450 eV. Broyden Fletcher Goldfarb Shanno (BFGS) geometry optimization method was used to find the lowest energy structure. The k-point is set to 11 × 11 × 6 and 3 × 3 × 1 based on Monkhorst-Pack method for the Brillouin zone sampling of unit cell and surface, respectively. A vacuum layer was built with the thickness of 15 Å to ensure the negligible interaction along Z axis. The convergence standard for total energy, maximum force, maximum stress, maximum displacement, self-consistent field (SCF)

were 1.0×10^{-5} eV/atom, 0.03 eV/Å, 0.05 GPa, 0.001 Å, and 1×10^{-6} eV/atom. The unit cell of hcp Ru was optimized according to the computational methods mentioned above firstly. The optimized lattice parameters of Ru are a = b = 2.719 Å and c = 4.284 Å, which are close to the experimental results (a = b = 2.751 Å and c = 4.282 Å).

1.6. Synthesis

Preparation of ruthenium nanoparticles supported on CNTs (Ru/C)

Ruthenium nanoparticles supported on CNTs were synthesized by an ethanol reduction method. Firstly, 0.4 mmol $RuCl_3$ in 100 mL ethanol was refluxed at 110 ºC for 1 h in an oil bath under magnetic stirring. Then, 200 mg CNTs was dispersed in ethanol solution by sonication for 1h and then injected into the pre-heated reaction flask. Upon the temperature of the solution stabilized at 110 ºC, 6 mL NaOH in ethanol (0.2 M) was injected quickly. The flask was capped and maintained at 110 ºC for 2h. Then, extra 0.2 mmol 0.2 M NaOH was injected into the reaction flask to assure complete reduction of Ru^{3+} ions. The solution was further refluxed for another 30 min and the nanocomposites was precipitated by centrifugation at 8,000 rpm for 10 min and dried in vacuum overnight. After annealed under H_2/Ar mixed-gas at 450 ºC for 1h in a tube furnace, crystalline Ru nanoparticles on CNTs were obtained, which was labeled as Ru/C.

The synthesis of nitrogen and Pt doped Ru nanoparticles: Ru@N, Ru@Pt, (Ru-N)@Pt and (Ru@Pt)-N NPs

Pt doped Ru NPs on CNTs were synthesized by following a procedure adapted from a prior report. Briefly, 20 mg Ru/C were dispersed in 40 mL aqueous ethanol solution ($EtOH/H_2O$ = 1 v/v) by sonication for 1h and then 30 mL 50 mmol chloroplatinic acid hexahydrate solution ($H_2PtCl_6.H_2O$) were transferred into the mixture. After stirring in a water bath at 0 °C for 3h, 1.6 mL 0.05mol/L $NaBH_4$ in DI water at 0 °C were added into the above reaction flask. One hour later, the final product was collected by centrifugation at 8,000 rpm for 10 min and dried overnight, which was labeled as Ru@Pt. The prepared Ru@Pt NPs were further annealed in ammonia gas at 250 ºC for 8 hours to obtain (Ru@Pt)-N NPs. Alternatively, 20 mg Ru@/C were first annealed in ammonia gas at 250 ºC for 8 hours to obtain Ru@N samples. Then Pt was deposited on Ru@N samples by following the procedure described above, to obtained N and Pt co-doped Ru nanoparticles, which are denoted as (Ru-N)@Pt NPs.

2. Supplementary Figures and Tables

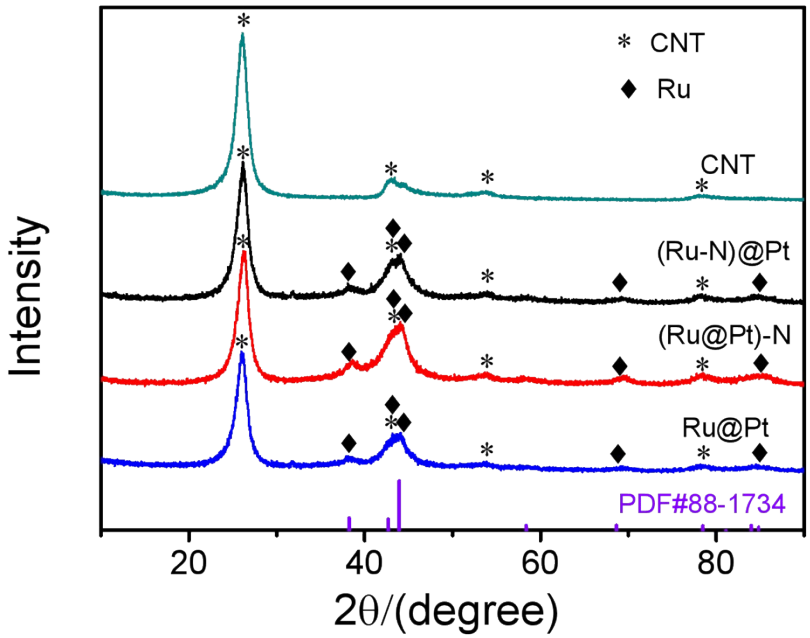

Fig. S1. XRD pattern of (Ru@Pt)-N, (Ru-N)@Pt and Ru@Pt at the ammonia temperature of 250 °C as well as CNT.

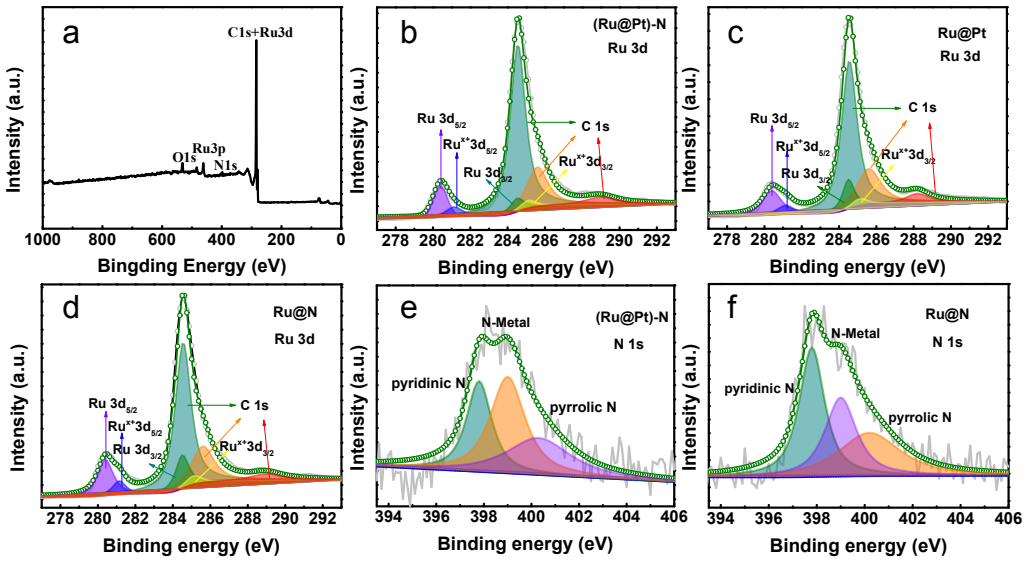

Fig. S2. (a) XPS survey spectra of as-prepared (Ru-N)@Pt. (b-d) Ru 3*d* spectra of (Ru@Pt)-N, Ru@Pt and Ru@N, respectively. (e, f) N 1*s* spectra of (Ru@Pt)-N and Ru@N, respectively. Gray curves are experimental data, shaded peaks are deconvolution fits, and green curves are the sum of the fits.

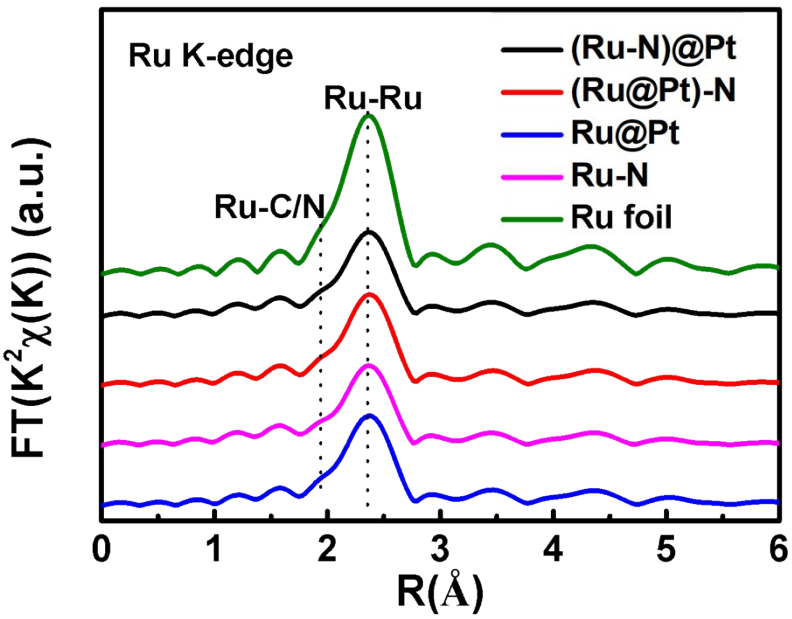

Fig. S3. Fourier transform (FT) of the k^2-weighted Ru K-edge of (Ru-N)@Pt, (Ru@Pt)-N, Ru@Pt, Ru@N and Ru foil.

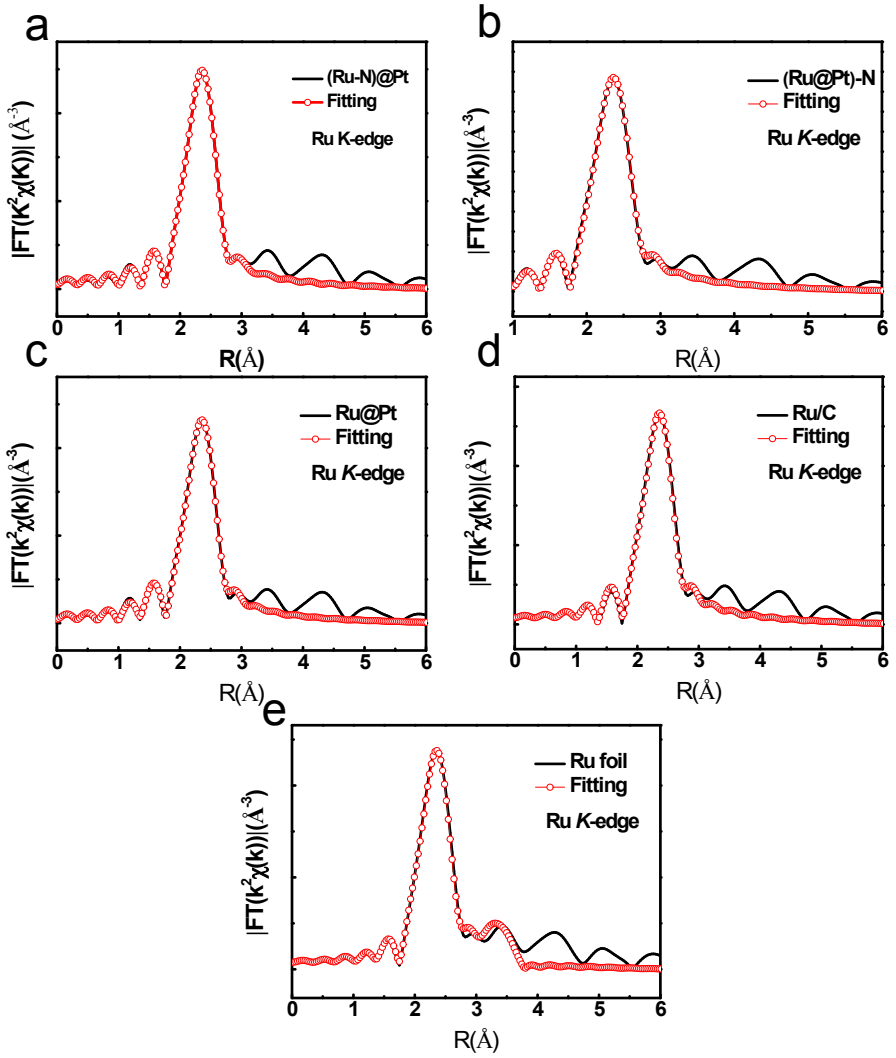

Fig. S4. The corresponding EXAFS fitting curves and raw data of Ru K-edge in R space for(Ru-N)@Pt, (Ru@Pt)-N, Ru@Pt, Ru/C and Ru foil, respectively.

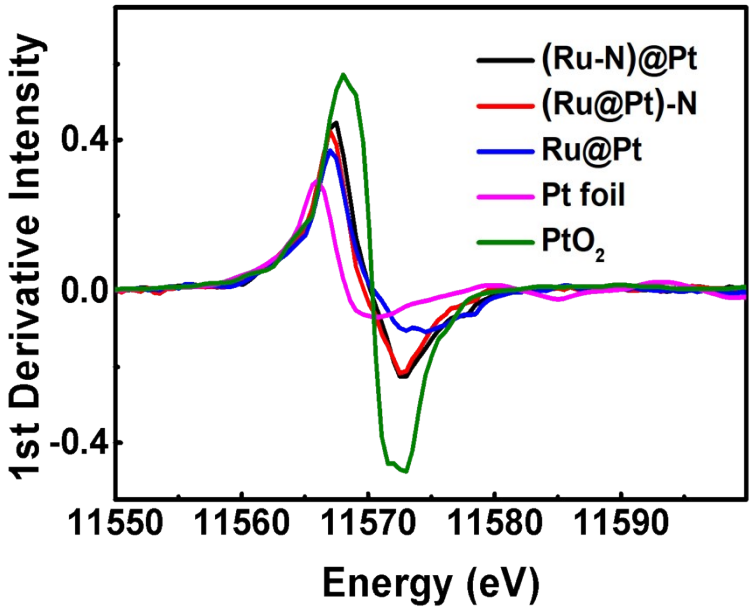

Fig. S5. The first derivative of the XANES spectra at Pt L_3-edge.

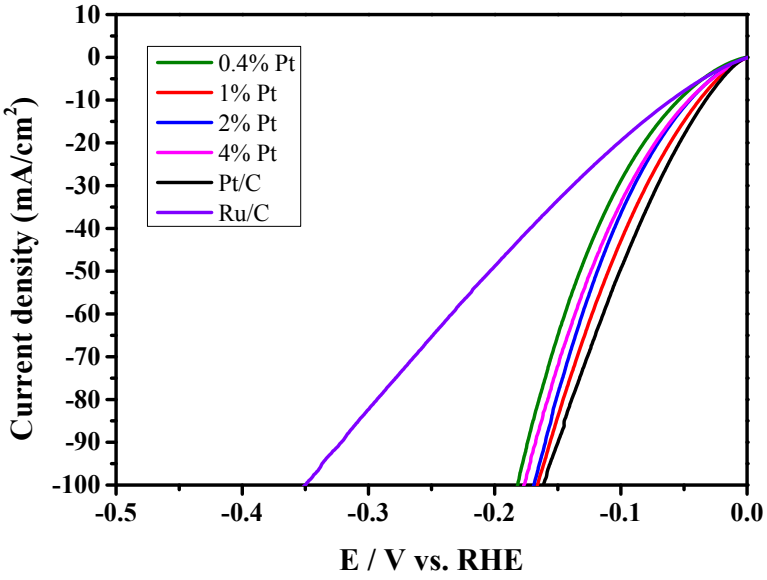

Fig. S6. Linear sweep polarization curves of Pt/C, Ru/C and (Ru-N)@Pt with varied Pt contents.

Turnover Frequency Calculations.

The number of active sites was quantified by the cyclic voltammetry (CV) method proposed by Hu and co-workers.[7] All CV measurements were conducted in the potential range of 0-1.25 V vs. RHE at a fixed scan rate of 50 mV s^{-1} in 0.5 M H_2SO_4 solution (pH = 0). The surface charge (Qs) was then calculated to be half of the integrated charge over the whole potential range.

The TOF value was calculated based on the number of active sites for each catalyst (considering the total metal loading in the catalyst) using the following formula:[7]

$$TOF(s^{-1}) = (j \times A)/(2 \times F \times n)$$

where j (A. cm^{-2}) is the current density at a given overpotential, A=0.196 cm^2 is the geometric surface area of the electrode, F=96500 C mol^{-1} stands for the Faraday constant, and n (mol)=Qs/F is the number of active sites.

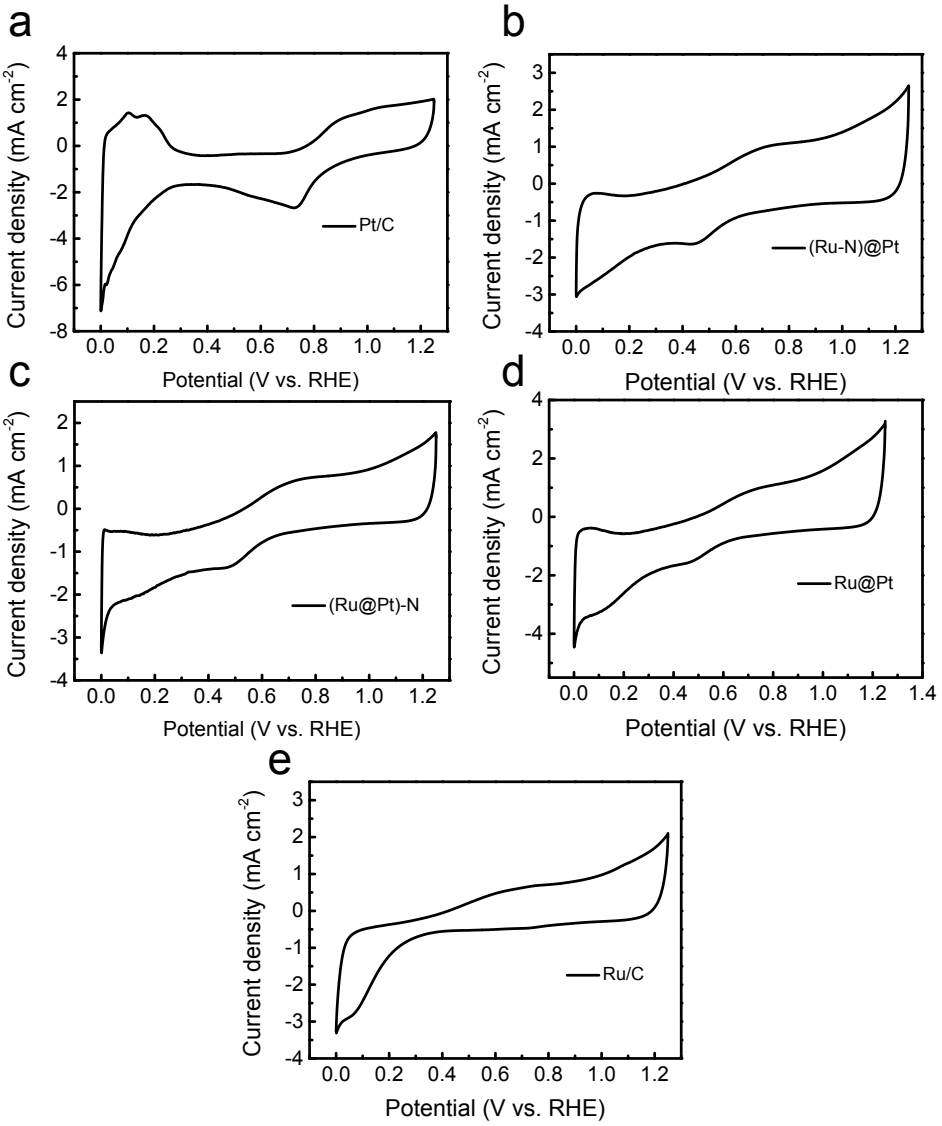

Fig. S7. The cyclic voltammograms (CV) curves of Pt/C, (Ru-N)@Pt, (Ru@Pt)-N, Ru@Pt and Ru/C in 0.5 M H_2SO_4 solution with a scan rate of 50 $mV \cdot s^{-1}$ and a rotation speed of 1600 rpm.

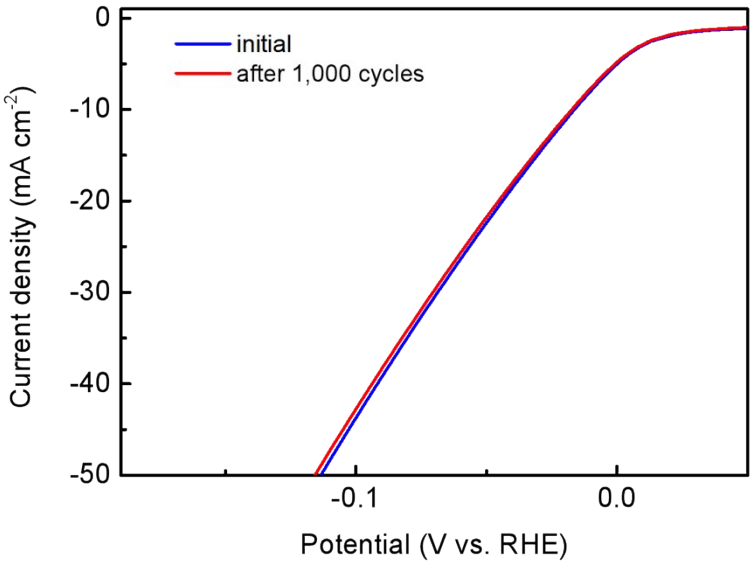

Fig. S8. Polarization curves for (Ru-N)@Pt before and after 1000 cycles with a scan rate of 100 mV s^{-1} between +0.20 and −0.20 V.

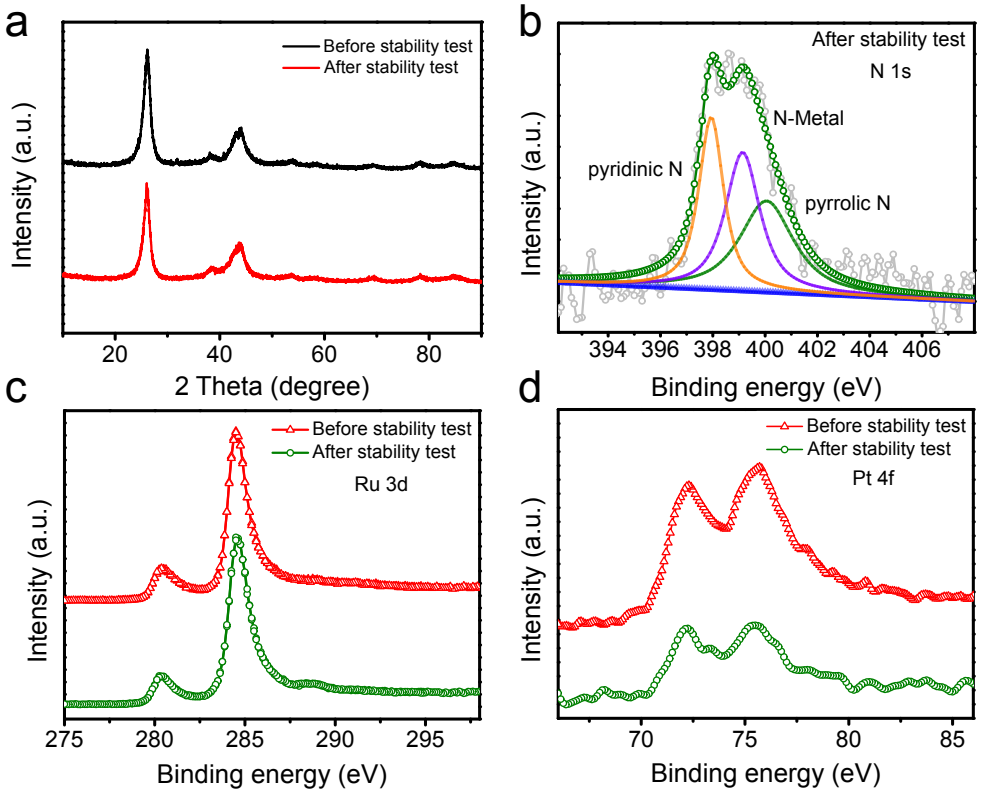

Fig. S9. (a) XRD patterns of (Ru-N)@Pt before and after long-time test. (b) N 1*s* spectra of (Ru-N)@Pt after stability test. (c-d) Ru 3*d* and Pt 4*f* spectra of (Ru-N)@Pt before and after stability test.

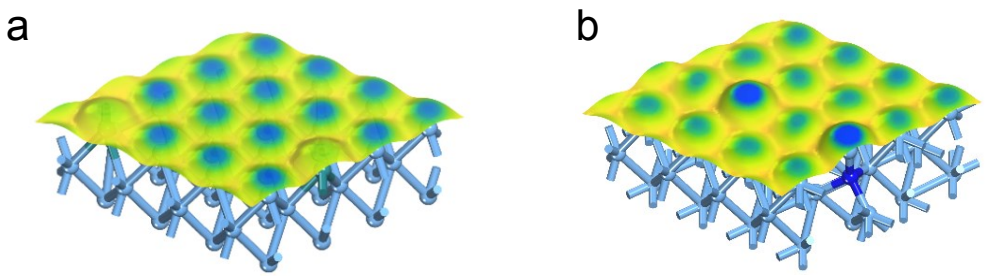

Fig. S10. The surface electrostatic potential maps based on the electron density difference of (a) Ru@Pt and (b) Ru-N

Fig. S11. The relative energy diagram along the water adsorption and water dissociation processes on both Ru@Pt (top) and Ru-N (bottom) surface with relative structure information.

Fig. S12. The 3*d* band PDOS of Ru sites on (a) Ru@Pt and (b) Ru-N surfaces before and after water adsorption. The right section adds the PDOS of O *p* band in adsorbed H_2O.

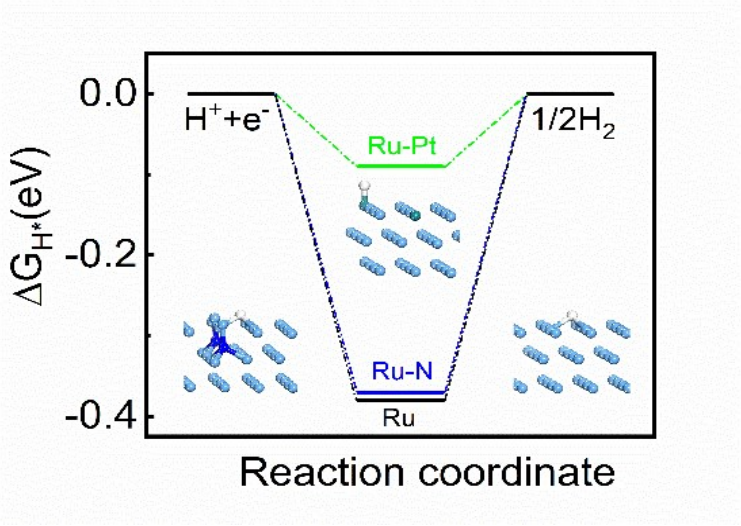

Fig. S13. The Gibbs free energy diagram of adsorbed H.

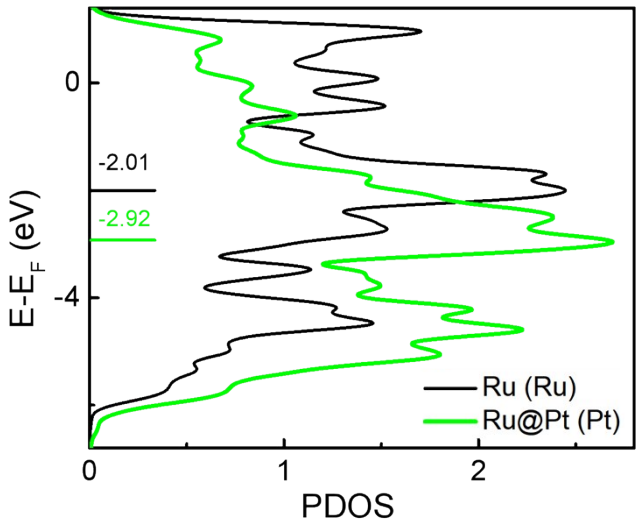

Fig. S14. The d band PDOS of active Ru site on Ru surface and active Pt site on Ru@Pt surface for H adsorption and desorption.

Table S1 Atomic ratio of catalysts obtained from ICP-AES and XPS.

Sample	XPS Surface composition (atomic %)			
	C	N	Ru	Pt
(Ru-N)@Pt	92.08	2.21	5.55	0.16
(Ru@Pt)-N	92.66	1.54	5.65	0.15
Ru@Pt	93.96	-	5.82	0.22
Ru@N	92.54	1.66	5.80	-
	ICP-Mass Bulk Composition (weight %)			
(Ru-N)@Pt			6.96	2.05

Table S2 Structural parameters of the samples obtained from EXAFS fitting.

Sample	Bond type	N	R (Å)	ΔE_0 (eV)	$\sigma^2 \times 10^3$ (Å^2)	R-factor
Ru-foil	Ru-Ru	12.0	2.67	-5.3	3.3	0.013
	Ru-Ru	6.0	3.79	-3.3	4.4	
(Ru-N)@Pt	Ru-C	3.0	2.02	3.7	8.0	0.006
	Ru-N	3.4	2.17	-2.5	8.0	
	Ru-Pt	5.2	2.42	23.0	14.8	
	Ru-Ru	8.0	2.67	-2.5	4.3	
(Ru@Pt)-N	Ru-C	3.0	2.02	0.8	9.0	0.004
	Ru-N	1.2	2.17	-5.6	11.0	
	Ru-Pt	5.3	2.43	0.6	14.0	
	Ru-Ru	5.8	2.69	0.09	3.1	
Ru/C	Ru-C	2.0	2.00	-14.0	9.0	0.008
	Ru-Ru	6.9	2.67	-4.3	3.5	
Ru@Pt	Ru-C	3.0	2.02	-5.3	9.0	0.003
	Ru-Pt	3.1	2.43	-0.1	11.4	

Ru-Ru	5.5	2.69	-1.8	3.6

N, coordination number; R, distance between absorber and backscatter atoms; ΔE, inner potential correction to account for the difference in the inner potential between the sample and the reference compound. σ^2, Debye–Waller factor; S_0^2 fitting from Ru sample defined as 0.85.

The EXAFS simulations above are based on the following equation:

$$\chi(k) = \sum_j \frac{N_j S_0^2 F_j(k)}{kR_j^2} \exp[\ 2k^2\sigma_j^2] \exp[\frac{2R_j}{\lambda(k)}] \sin[2kR_j + \phi_j(k)]$$

N_j is the number of neighbors in the jth atomic shell, S_0^2 is the amplitude reduction factor, $F_j(k)$ is the effective curved-wave backscattering amplitude, R_j is the distance between the X-ray absorbing central atom and the atoms in the jth atomic shell (backscatterer), σ_j is the Debye-Waller parameter of the jth atomic shell (variation in the distances around the average R_j), λ is the mean free path in Å, $\phi_j(k)$ is the phase shift (including the phase shift for each shell and the total central atom phase shift). The functions $F_j(k)$, λ and $\phi_j(k)$ were calculated with the ab initio code FEFF8.2.[8] The simulation details are given below. The coordination numbers of the model samples (Ru foil) was fixed as the standard values. The obtained $S0^2$ of Ru foil was 0.85 and it was fixed in the subsequent fitting of Ru K-edge data for the (Ru-N)@Pt, (Ru@Pt)-N, Ru/C and Ru@Pt catalysts. In contrast, the internal atomic distances R, the edge-energy shift ΔE_0 and Debye-Waller factor σ^2 were permitted to work separately. The obtained

parameters of the Ru K-edge are listed in Table S2, and the curve-fitting results are shown in Figure S4.

Table S3. HER performances of (Ru-N)@Pt and other reported electrocatalysts in alkaline media.

Catalyst	**Electrolyte**	**η(mV) at j=10 mA cm^{-2}**	**Durability**	**Electrolyte**
(Ru-N)@Pt	1.0M KOH	15	58h	This work
Pt_3Ni_2-NWs-S/C	1.0M KOH	42	5h	[9]
Pt_3Ni	0.1M KOH	65(η_5)	-	[10]
Pt-Ni(N)	1.0M KOH	13	10h	[11]
Pt-Ni ASs	1.0M KOH	27.7	10000 cycle	[12]
Pd-Pt	1.0M KOH	70	2h	[13]
Ru@C_2N	1.0M KOH	17	10000 cycle	[14]
PtNi-O/C	1.0M KOH	39.8	10h	[15]
Hcp Pt-Ni	0.1M KOH	65	1h	[16]
Ru-Ni SNs	0.1M KOH	42.7	-	[17]
PtRu@RFCS	0.5M H_2SO_4	19.5	-	[18]
Ni@Ni_2P-Ru HNRs	1.0M KOH	31	1000 cycle	[19]

Reference

1. H.S. Yu, X.J. Wei, J. Li, S.Q. Gu, S. Zhang, L.H. Wang, J.Y. Ma, L.N. Li, Q. Gao, R. Si, F.F. Sun, Y. Wang, F. Song, H.J. Xu, X.H. Yu, Y. Zou, J.Q. Wang, Z. Jiang, Y.Y. Huang, *Nucl Sci Tech*, 2015, **26**.
2. B. Ravel and M. Newville, *J. Synchrotron. Radiat.*, 2005, **12**, 537-541.
3. J.J. Rehr, J. Muster de Leon, S.I. Zabinsky, R.C. Albersl, *J. Am. Chem. Soc*, 1991, **113**, 5135-5140,.
4. J. Mustre de Leon, J. J. Rehr, S. I. Zabinsky and R. C. Albers, *Phys. Rev. B, Condensed matter*, 1991, **44**, 4146-4156.
5. T. Ressler, *Le Journal de Physique IV*, 1997, **7**, C2-269-C262-270.
6. S. J. Clark, M. D. Segall, C. J. Pickard, P. J. Hasnip, M. I. J. Probert, K. Refson and M. C. Payne, *Zeitschrift für Kristallographie - Crystalline Materials*, 2005, **220**.
7. D. Merki, S. Fierro, H. Vrubel and X. Hu, *Chem. Sci.*, 2011, **2**, 1262-1267.
8. J. Ge, D. He, W. Chen, H. Ju, H. Zhang, T. Chao, X. Wang, R. You, Y. Lin, Y. Wang, J. Zhu, H. Li, B. Xiao, W. Huang, Y. Wu, X. Hong and Y. Li, *J. Am. Chem. Soc.*, 2016, **138**, 13850-13853.
9. P. Wang, X. Zhang, J. Zhang, S. Wan, S. Guo, G. Lu, J. Yao and X. Huang, *Nat Commun*, 2017, **8**, 14580.
10. C. Chen, Y. Kang, Z. Huo, Z. Zhu, W. Huang, H. L. Xin, J. D. Snyder, D. Li, J. A. Herron, M. Mavrikakis, M. Chi, K. L. More, Y. Li, N. M. Markovic, G. A. Somorjai, P. Yang and V. R. Stamenkovic, *Science*, 2014, **343**, 1339-1343.
11. Y. Xie, J. Cai, Y. Wu, Y. Zang, X. Zheng, J. Ye, P. Cui, S. Niu, Y. Liu, J. Zhu, X. Liu, G. Wang and Y. Qian, *Advanced materials*, 2019, **31**, e1807780.
12. Z. Zhang, G. Liu, X. Cui, B. Chen, Y. Zhu, Y. Gong, F. Saleem, S. Xi, Y. Du, A. Borgna, Z. Lai, Q. Zhang, B. Li, Y. Zong, Y. Han, L. Gu and H. Zhang, *Adv. Mater.*, 2018, **30**, e1801741.
13. J. Fan, K. Qi, L. Zhang, H. Zhang, S. Yu and X. Cui, *ACS Applied Materials & Interfaces*, 2017, **9**, 18008-18014.
14. J. Mahmood, F. Li, S. M. Jung, M. S. Okyay, I. Ahmad, S. J. Kim, N. Park, H. Y. Jeong and J. B. Baek, *Nat. Nanotech.*, 2017, **12**, 441-446.
15. Z. Zhao, H. Liu, W. Gao, W. Xue, Z. Liu, J. Huang, X. Pan and Y. Huang, *J. Am. Chem. Soc.*, 2018, **140**, 9046-9050.
16. Z. Cao, Q. Chen, J. Zhang, H. Li, Y. Jiang, S. Shen, G. Fu, B. A. Lu, Z. Xie and L. Zheng, *Nat Commun*, 2017, **8**, 15131.
17. J. Ding, Q. Shao, Y. Feng and X. Huang, *Nano Energy*, 2018, **47**, 1-7.
18. K. Li, Y. Li, Y. Wang, J. Ge, C. Liu and W. Xing, *Energy. Environ. Sci.*, 2018, **11**, 1232-1239.
19. Y. Liu, S. Liu, Y. Wang, Q. Zhang, L. Gu, S. Zhao, D. Xu, Y. Li, J. Bao and Z. Dai, *J. Am. Chem. Soc.*, 2018, **140**, 2731-2734.